

Subtropical sea-surface warming and increased salinity during Eocene Thermal Maximum 2

Dustin T. Harper¹, Richard Zeebe², Bärbel Hönisch³, Cindy D. Schrader⁴, Lucas J. Lourens⁴, and James C. Zachos¹

¹Department of Earth and Planetary Sciences, University of California–Santa Cruz, 1156 High Street, Santa Cruz, California 95064, USA ²School of Ocean and Earth Science and Technology, University of Hawaii at Manoa, 1000 Pope Road, MSB 507, Honolulu, Hawaii 96822, USA

³Department of Earth and Environmental Sciences and Lamont-Doherty Earth Observatory of Columbia University, Geoscience Building, P.O. Box 1000, Palisades, New York 10964, USA

⁴Faculty of Geosciences, Utrecht University, 3584 CD Utrecht, Netherlands

ABSTRACT

Eocene Thermal Maximum 2 (ETM-2; ca. 54.2 Ma) represents the second largest of the major Eocene hyperthermals, yet comparatively little is known about the scale and rate of climatic change for key regions. Here we provide the first detailed records of subtropical sea-surface warming and salinization for ETM-2 at two subtropical locations, Ocean Drilling Program Sites 1209 (North Pacific) and 1265 (South Atlantic). Coupled planktic foraminiferal Mg/Ca and δ^{18} O indicate 2–4 °C of rapid warming and local salinization of ~1–2 ppt at both sites. The increase in sea-surface temperature is equivalent to anomalies reported from higher latitude sites, and is consistent with theory on the expected pattern of spatial temperature response to greenhouse gas forcing in an ice-free world (i.e., no ice-albedo feedback). Similarly, the observed salinization is consistent with the hypothesis of enhanced meridional vapor transport and increased subtropical aridity in a warmer world.

INTRODUCTION

The early Eocene hyperthermals represent potential calibration points for establishing the response of global and regional warming and shifts in the hydrologic cycle to past changes in greenhouse gas (GHG) forcing because they represent transient and extreme warming events. The magnitude of warming (4–8 °C; e.g., Dunkley Jones et al., 2013) during the largest hyperthermal, the Paleocene–Eocene Thermal Maximum (PETM; ca. 56 Ma), and evidence for intensification of the hydrologic cycle (e.g., Schmitz and Pujalte, 2007) are roughly within projections given the estimates of GHG forcing and PETM climate sensitivity (PALEOSENS Project Members, 2012; Kiehl and Shields, 2013).

Subsequent but smaller hyperthermals represent additional climate sensitivity calibration points. The Eocene Thermal Maximum 2 (ETM-2; ca. 54 Ma) followed the PETM by 1.8-2.0 m.y., and was characterized by surface- and deep-ocean warming (Lourens et al., 2005; Sluijs et al., 2009; Stap et al., 2009) that was approximately half that of the PETM. The magnitude of the accompanying carbon isotope excursion (CIE, -1%0 to -1.5%0 in benthic foraminifera; e.g., Stap et al., 2010a; Fig. DR1 in the GSA Data Repository¹) and dissolution horizons

¹GSA Data Repository item 2018045, supplemental information including methodological details and figures that support the discussion, is available online at http://www.geosociety.org/datarepository/2018/ or on request from editing@geosociety.org

(Lourens et al., 2005; Nicolo et al., 2007; Stap et al., 2009; Westerhold et al., 2011) indicates a global carbon cycle perturbation that is also approximately half that of the PETM, although this has yet to be adequately constrained by independent observations or modeling.

In addition to warming, the hyperthermals are also characterized by a mode shift, or intensification, of the hydrologic cycle. In the case of the PETM this includes widespread evidence of increased intensity and/or frequency of extreme precipitation events and drought in continental settings (Schmitz and Pujalte, 2007; Kraus and Riggins, 2007; Foreman et al., 2012), and changes in runoff and/or precipitation and evaporation (P-E) in marine settings (Zachos et al., 2003, 2006; Tripati and Elderfield, 2004; Nicolo et al., 2007; Tipple et al., 2011). In particular, open-ocean P-E, as inferred from changes in sea-surface salinity (Δ SSS), appears to have declined in the subtropics, and increased in high latitudes. Similarly, cursory evidence for intensification of the hydrologic cycle has been documented for ETM-2 in the Arctic and North America (Sluijs et al., 2009; Abels et al., 2012), but few other locations.

Previous attempts to quantify ETM-2 warming have been limited to a few planktic $\delta^{18}O$ records that show modest (negative) anomalies (Lourens et al., 2005; Stap et al., 2010a), possibly due to the influence of competing environmental factors, such as higher SSS and acidification (e.g., Spero et al., 1997), both of which

would be consistent with a global carbon cycle perturbation. Subtropical salinization would be expected due to increased subtropical evaporation and transport of $^{18}\text{O-depleted}$ water vapor poleward on a global scale (e.g., Roberts et al., 2011; Tindall et al., 2010). To circumvent this, additional proxies such as Mg/Ca are required to constrain sea-surface temperature (SST), which, with adjustments for pH (Evans et al., 2016), could then allow for estimation of changes in local sea-surface $\delta^{18}\text{O}_{\text{seawater}}$ and thus SSS (e.g., Zachos et al., 2003).

To assess whether the magnitude of ETM-2 warming was globally uniform in the absence of an ice-albedo feedback (e.g., Kiehl and Shields, 2013), and to test if regional P-E declined in the subtropics due to increased meridional vapor transport consistent with GHG warming (Carmichael et al., 2015), we applied coupled $\delta^{18}O$ and Mg/Ca paleothermometry in planktic foraminifera from Ocean Drilling Program (ODP) Sites 1209 and 1265 to establish low- to mid-latitude SST and SSS anomalies.

METHODS

Specimens of Acarinina soldadoensis, a planktic foraminifera species that likely hosted photosymbionts and thus resided in the photic zone (e.g., Pearson et al., 1993), were collected from the 250-355 µm sieve size fraction at 3-5 k.y. resolution from ODP Sites 1209 and 1265, where ETM-2 is tightly constrained by carbon isotope and cycle stratigraphy (Lourens et al., 2005; Westerhold et al., 2007; Gibbs et al., 2012). Trace element ratios (e.g., Mg/Ca, Sr/Ca, Al/Ca, Ti/Ca) of oxidatively reductively cleaned specimens (10-20 shells) were measured by inductively coupled plasma-mass spectrometry following the methodology of Brown et al. (2011) with an interrun precision for Mg/ Ca of <3% (2 standard deviation). Stable isotope analyses (δ¹³C, δ¹⁸O, Vienna Peedee belemnite) were performed on shells from the same samples via isotopic ratio mass spectrometry with an interrun precision for δ^{13} C and δ^{18} O < 0.1% (2 relative standard deviation, RSD)

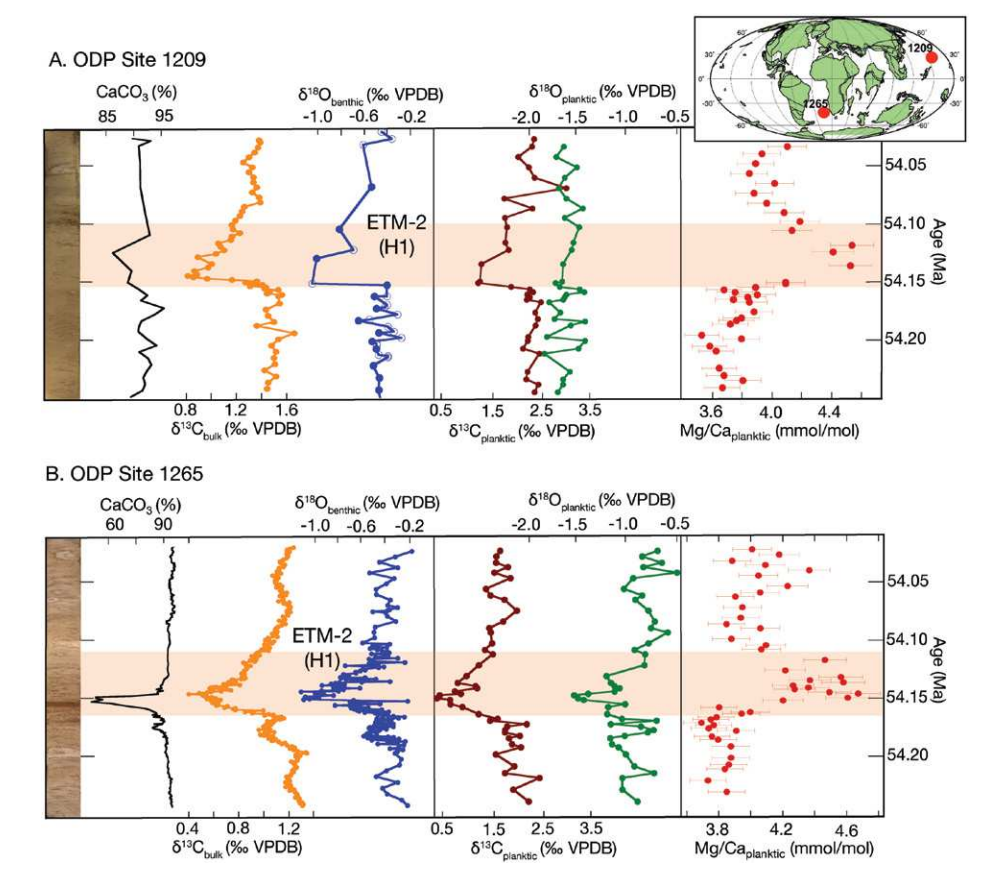


Figure 1. A: Bulk CaCO $_3$ concentration (black line, this study) and δ^{13} C (orange symbols, Gibbs et al., 2012), benthic (*Nuttallides truempyi*; blue symbols) δ^{18} O (McCarren, 2009; this study = open symbols), planktic (*Acarinina soldadoensis*) δ^{13} C (burgundy symbols), δ^{18} O (green symbols) and Mg/Ca (red symbols) (this study) for Ocean Drilling Program (ODP) Site 1209 (~28°N paleolatitude; van Hinsbergen et al., 2015). Data are plotted versus absolute age using the age model of Lauretano et al. (2016). The age model for Site 1209 was generated by tying the bulk δ^{13} C record at Site 1209 to bulk δ^{13} C at Site 1265. Inset: The site map displays the continental configuration at 54.0 Ma and indicates the paleolocations of Sites 1209 and 1265. The pink shaded bar highlights ETM-2 (or the H1 event). B: ODP Site 1265 (42°S paleolatitude). Symbols as in A except CaCO $_3$ data (% and δ^{13} C; black line and orange symbols, respectively) are from Stap et al. (2009) and benthic (*N. truempyi*, blue symbols) δ^{18} O data are from Stap et al. (2010b).

and <0.16% (2 RSD), respectively. A %CaCO₃ record was also generated for ODP Site 1209 via coulometric analysis. In addition, we compiled previously published bulk CaCO₃ (% and δ^{13} C) and benthic foraminiferal δ^{13} C and δ^{18} O for Site 1265 (Stap et al., 2009, 2010a, 2010b) and bulk δ^{13} C and benthic foraminiferal δ^{13} C and δ^{18} O for Site 1209 (Gibbs et al., 2012; McCarren, 2009). Details of all analytical and numerical methods are provided in the Data Repository.

From the coupled planktic Mg/Ca and $\delta^{18}O$ data (Fig. 1), SST and SSS anomalies were computed (Fig. 2) following the method of Zachos et al. (2003), but accounting for additional recently discovered proxy sensitivities. Specifically, the exponential constant of the Mg/Ca proxy calibration (A value; see Equation 3 in the Data Repository) is potentially sensitive to Mg/Ca_{scawater} (Evans et al., 2016). In order to account for this sensitivity, we applied a range of constants (A values from 0.05 to 0.09) that encompass the error in Mg/Ca temperature regression fits for potential Mg/Ca_{scawater} values

of the early Eocene (see the Data Repository; Evans et al., 2016) that contribute to the uncertainty in Δ SST (i.e., ± 1 °C). Furthermore, Evans et al. (2016) observed a pH effect on Mg/Ca that they quantified using a logistic fit to trends

in field and laboratory data (Equation 1 in the Data Repository), although they could not statistically rule out a linear fit (Equation 2 in the Data Repository). Using a $\delta^{11}B$ -based estimate of ΔpH (Penman et al., 2014) for the PETM, Evans et al. (2016) applied a pH correction to planktic δ^{18} O and Mg/Ca data of Zachos et al. (2003) to highlight the significance of this effect. Because ΔpH has not yet been established for ETM-2, we apply a ΔpH of -0.05 pH units, estimated using Long-Term Ocean-Atmosphere-Sediment Carbon Cycle Reservoir (LOSCAR) carbon-cycle simulation of the event, as constrained by observations of the magnitude of the CIE, ΔSST, and changes in the carbonate compensation depth (CCD) (see the Data Repository). Applying both the logistic and linear pH adjustments, the pH effect on our Mg/Ca-ΔSST is <-0.1 °C (Fig. DR3). Scaling the Site 1209 δ^{11} B-based PETM ΔpH (Penman et al., 2014) to ETM-2 using the planktic CIE recorded for each event (see the Data Repository) leads to a larger ΔpH (-0.11 pH units), although the added effect on our results is minimal (<0.1 °C decrease in Δ SST and <0.2 ppt decrease in Δ SSS; Fig. DR3).

Planktic $\delta^{18}O$ values are also adjusted with LOSCAR-based ΔpH (-0.05 pH units) following the *Globigerina bulloides* relationship initially ascribed to a [CO₃²⁻] effect on $\delta^{18}O$ by Spero et al. (1997) (i.e., -2.51% per pH unit), before estimating and removing the Mg/Ca-based temperature influence to determine $\delta^{18}O_{\text{seawater}}$. The residual shifts in $\delta^{18}O_{\text{seawater}}$ are then converted to Δ SSS using 0.25%–0.50% per ppt from Zachos et al. (2003). This approach assumes (1) the complete absence of ice sheets to influence $\delta^{18}O_{\text{seawater}}$, and (2) that the state of foraminifera preservation is uniform on short length scales, where lithology (i.e., %CaCO₃) is relatively invariant (Fig. 1).

RESULTS

At both sites, Mg/Ca increases by ~25% during the CIE (Fig. 1). Given the long residence times of Mg and Ca in seawater (>1 m.y.),

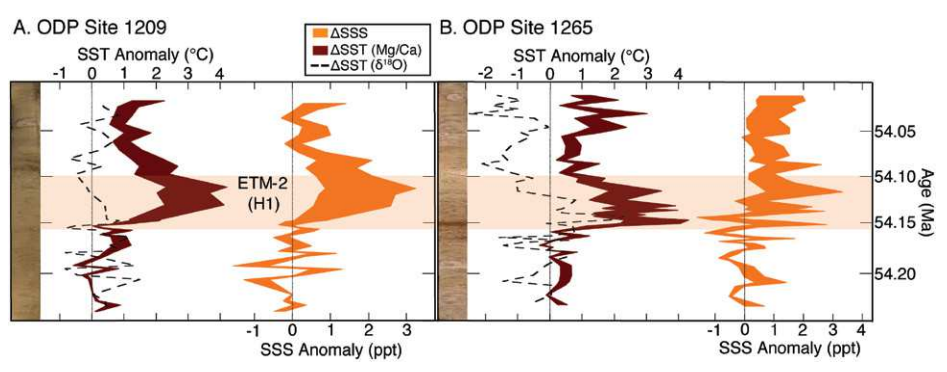


Figure 2. A: Eocene Thermal Maximum 2 (ETM-2) (or the H1 event) sea-surface temperature (SST) and sea-surface salinity (SSS) anomalies from Ocean Drilling Program (ODP) Site 1209. $\delta^{18}\text{O-based SST}$ anomaly is pH adjusted. Mg/Ca-based SST and temperature-adjusted $\delta^{18}\text{O}_{\text{residual}}$ based SSS anomalies are generated following the methodology outlined in the text and in the Data Repository (see footnote 1). B: ODP Site 1265.

Mg/Ca_{seawater} should have remained constant over the duration of the study interval (~200 k.y.); thus, the Mg/Ca anomalies must reflect Δ SST. During the CIE of ETM-2, planktic $\delta^{18}O$ values decrease by <0.5% during the CIE at South Atlantic ODP Site 1265, but at Pacific Site 1209 show little to no decrease beyond background variability. In contrast, benthic δ^{18} O data show a similar 0.6%o-0.7%o decrease at both locations (Fig. 1; Stap et al., 2010b), suggesting similar warming of the deep sea. Surface-ocean CIEs of ~-1.5% are recorded in mixed-layer planktic foraminifera at both sites (Fig. 1). The %CaCO₃ decreases by ~40% at Site 1265 (Stap et al., 2009) and by ~5% at Site 1209 (this study) during the CIE (Fig. 1).

ΔSST AND ΔSSS FROM THE SUBTROPICS DURING ETM-2

We focus on establishing anomalies instead of absolute SST and SSS, because recrystallization of planktic foraminifera in carbonate-rich pelagic oozes can shift δ^{18} O substantially (Pearson et al., 2001). Any overprint of δ^{18} O, however, should be uniform over the short length scales studied here, and features such as anomalies (and cycles) are typically preserved (Kozdon et al., 2013). In contrast, Mg/Ca seems to be minimally affected by recrystallization in relatively closed systems such as the low-porosity pelagic muds at Sites 1209 and 1265 (Kozdon et al., 2013; Edgar et al., 2015). Dissolution, however, tends to decrease Mg/Ca and increase δ^{18} O in foraminiferal calcite (Dekens et al., 2002). Combining the dissolution sensitivity of the modern foraminifera G. ruber (Dekens et al., 2002) with our simulated CCD response for ETM-2 (Fig. DR2) translates to a potential Mg/Ca decrease due to dissolution of 1%-3% and 2%-6% in the Pacific and Atlantic, respectively. In terms of SST, this would dampen ETM-2 warming by <0.5 °C in the Pacific, and <1 °C in the Atlantic. In contrast, $\delta^{18}O$ dissolution sensitivity might suggest a potential increase in foraminiferal δ^{18} O of <0.04 ‰ and <0.08‰ for the Pacific and Atlantic, respectively. This magnitude of δ^{18} O enrichment would tend to amplify our calculated \triangle SSS by only <0.25 ppt, for both sites. However, estimates of the effect of dissolution on our results are likely extremes, as the depthdependent dissolution effect probably overcompensates for actual dissolution (e.g., Hönisch et al., 2013). Furthermore, the muted δ^{18} O temperature signal is observed at both sites, which exhibit variable decreases in %CaCO₃.

In general, Mg/Ca suggest a similar degree of warming in the equatorial Pacific and South Atlantic during ETM-2. The $\delta^{18}O$ anomalies, in contrast, are small and unequal, indicating local salinity-related anomalies in $\delta^{18}O_{\text{seawater}}$. We find that the total rise in SST amounts to 2–4 °C during ETM-2 (Fig. 2) and residual shifts in $\delta^{18}O_{\text{seawater}}$ indicate an increase in SSS of +2 \pm 1

ppt at Site 1209 and $+1 \pm 1$ at 1265 (Fig. 2), suggesting increased subtropical aridity coincident with the warming.

DISCUSSION

The 2-4 °C warming in low to mid-latitudes established herein is similar in magnitude to bottom-water warming recorded by deep-sea benthic δ^{18} O (~3 °C; Stap et al., 2010b), where negligible changes in pH and salinity are predicted, by inference, in areas of bottom-water formation in the Southern Ocean and the Arctic (3–5 °C ΔSST; Sluijs et al., 2009). The spatial pattern of warming for ETM-2 is similar (albeit smaller in magnitude) to the pattern recorded by Mg/Ca and GDGT (glycerol dialkyl glycerol tetraethers) based temperature estimates during the PETM (e.g., Dunkley Jones et al., 2013) and expected pattern of warming in a largely ice-free world that lacks ice-albedo feedbacks (Kiehl and Shields, 2013).

Our finding of increased subtropical salinity during ETM-2 supports theoretical considerations of Eocene greenhouse warming effects on atmospheric vapor transport, ocean salinity, and $\delta^{18}O_{seawater}$. Simulations with isotope-enabled climate models (Roberts et al., 2011; Tindall et al., 2010) suggest relatively enhanced evaporation in the subtropics and net transport of ¹⁸O-depleted moisture poleward, raising both the salinity and $\delta^{18}O_{seawater}$ of subtropical surface waters. In one simulation involving the GISS (Goddard Institute for Space Studies) ModelE-R (Roberts et al., 2011), P-E decreases in the subtropical latitude bands from 15°S to 45°S, and from 10°N to 40°N, resulting in 0.5-2.0 ppt local increases in SSS, the largest increases occurring in the subtropical Pacific and the North Atlantic and the smallest in the equatorial Pacific. Similarly, the HadCM3 (Hadley Centre coupled atmosphereocean general circulation model) was used to simulate differences between preindustrial and Eocene $\delta^{18}O_{\text{seawater}}$ producing broadly similar results as the GISS ModelE-R, with some local differences in the Indian Ocean and North Atlantic Ocean basins (Tindall et al., 2010). It is interesting that near Site 1265, simulated changes in P-E appear to be small, and so the site would record a reduced $\delta^{18}O_{\text{seawater}}$ anomaly, consistent with our findings. While orbital forcing and ocean circulation might have contributed, the close covariation of SSS and SST with the CIE during the transient Eocene hyperthermals supports a primary feature of climate theory, that GHG warming drives increased meridional moisture transport, i.e., intensification of the hydrologic cycle (Carmichael et al., 2015).

Our estimate of surface salinization recorded during ETM-2 at Site 1209 is similar in magnitude to the original estimate of a 2–3 ppt increase for the PETM (Zachos et al., 2003). This original estimate was not adjusted for pH or for other effects on either $\delta^{18}O$ and Mg/Ca.

In order to compare the salinity anomalies for the PETM and ETM-2, we recalculated PETM Δ SST and Δ SSS using planktic Mg/Ca and δ ¹⁸O data from Zachos et al. (2003). Applying the same range in Mg/Ca temperature sensitivity (A values) as used for ETM-2 and adjusting for ΔpH using simulated LOSCAR Pacific surface PETM ΔpH (~-0.17 units; Zeebe et al., 2009), we estimate a salinity anomaly of 3 ± 2 ppt for the PETM at Site 1209 (Fig. DR4). We used the LOSCAR PETM ΔpH over the $\delta^{11}B$ -based PETM ΔpH to maintain consistency when comparing the SSS anomalies for the two events. The large uncertainty in the recalculated PETM ΔSSS reflects a broad range of possible Mg/Ca temperature sensitivities for the Eocene. When averages are compared, the PETM salinity anomaly at Site 1209 is slightly larger than the anomaly for ETM-2 (i.e., 3 ± 2 ppt for the PETM, and 2 ± 1 ppt for ETM-2; Fig. 2; Fig. DR4), as one would expect, due to the relatively larger perturbations in temperature and hydrological cycle during the PETM compared to ETM-2.

In summary, this study documents patterns of sea-surface warming and salinization of the subtropical (~28°N) Pacific and subtropical (~42°S) South Atlantic during ETM-2 that are consistent with theoretical predictions of the climatic response to GHG forcing, including globally uniform warming in the absence of ice-albedo feedback, a decrease in P-E, and a corresponding increase in SSS at low to mid-latitudes, suggesting enhanced meridional vapor transport.

ACKNOWLEDGMENTS

We thank Rob Franks, Dyke Andreasen, and Colin Carney for analytical support. We appreciate the feedback from Paul Wilson, Mark Leckie, and an anonymous reviewer. This research used samples from the International Ocean Discovery Project and was supported by the National Science Foundation (grants OCE16–57848 to Hönisch and OCE16–58023 to Zeebe and Zachos) and Netherlands Earth System Science Centre Gravitation Grant 024.002.001 (to Lourens and Schrader).

REFERENCES CITED

Abels, H.A., Clyde, W.C., Gingerich, P.D., Hilgen, F.J., Fricke, H.C., Bowen, G.J., and Lourens, L.J., 2012, Terrestrial carbon isotope excursions and biotic change during Palaeogene hyperthermals: Nature Geoscience, v. 5, p. 326–329, https://doi.org/10.1038/ngeo1427.

Brown, R.E., Anderson, L.D., Thomas, E., and Zachos, J.C., 2011, A core-top calibration of B/Ca in the benthic foraminifers *Nuttallides umbonifera* and *Oridorsalis umbonatus*: A proxy for Cenozoic bottom water carbonate saturation: Earth and Planetary Science Letters, v. 310, p. 360–368, https://doi.org/10.1016/j.epsl.2011.08.023.

Carmichael, M., et al., 2015, Insights into the early Eocene hydrological cycle from an ensemble of atmosphere-ocean GCM simulations: Climate of the Past Discussions, v. 11, p. 3277–3339, https://doi.org/10.5194/cpd-11-3277-2015.

Dekens, P.S., Lea, D.W., Pak, D.K., and Spero, H.J., 2002, Core top calibration of Mg/Ca in tropical foraminifera: Refining paleotemperature

- estimation: Geochemistry, Geophysics, Geosystems, v. 3, p. 1–29, https://doi.org/10.1029/2001GC000200.
- Dunkley Jones, T., Lunt, D.J., Schmidt, D.N., Ridgwell, A., Sluijs, A., Valdes, P.J., and Maslin, M., 2013, Climate model and proxy data constraints on ocean warming across the Paleocene–Eocene Thermal Maximum: Earth-Science Reviews, v. 125, p. 123–145, https://doi.org/10.1016/j.earscirev.2013.07.004.
- Edgar, K.M., Anagnostou, E., Pearson, P.N., and Foster, G.L., 2015, Assessing the impact of diagenesis on δ¹¹B, δ¹³C, δ¹⁸O, Sr/Ca and B/Ca values in fossil planktic foraminiferal calcite: Geochimica et Cosmochimica Acta, v. 166, p. 189–209, https://doi.org/10.1016/j.gca.2015.06.018.
- Evans, D., Wade, B.S., Henehan, M., Erez, J., and Müller, W., 2016, Revisiting carbonate chemistry controls on planktic foraminifera Mg/Ca: Implications for sea surface temperature and hydrology shifts over the Paleocene–Eocene Thermal Maximum and Eocene–Oligocene Transition: Climate of the Past, v. 11, p. 3143–3185, https://doi.org/10.5194/cpd-11-3143-2015.
- Foreman, B.Z., Heller, P.L., and Clementz, M.T., 2012, Fluvial response to abrupt global warming at the Palaeocene/Eocene boundary: Nature, v. 491, p. 92–95, https://doi.org/10.1038/nature11513.
- Gibbs, S.J., Bown, P.R., Murphy, B.H., Sluijs, A., Edgar, K.M., Pälike, H., and Zachos, J.C., 2012, Scaled biotic disruption during early Eocene global warming events: Biogeosciences, v. 9, p. 4679–4688, https://doi.org/10.5194/bg-9-4679 -2012.
- Hönisch, B., Allen, K.A., Lea, D.W., Spero, H.J., Eggins, S.M., Arbuszewski, J., Rosenthal, Y., Russell, A.D. and Elderfield, H., 2013, The influence of salinity on Mg/Ca in planktic foraminifers—Evidence from cultures, core-top sediments and complementary δ¹⁸O: Geochimica et Cosmochimica Acta, v. 121, p. 196–213, https://doi.org/10.1016/j.gca.2013.07.028.
- Kiehl, J.T., and Shields, C.A., 2013, Sensitivity of the Palaeocene–Eocene Thermal Maximum climate to cloud properties: Royal Society of London Philosophical Transactions, ser. A, v. 371, https://doi.org/10.1098/rsta.2013.0093.
- Kozdon, R., Kelly, D.C., Kitajima, K., Strickland, A., Fournelle, J.H., and Valley, J.W., 2013, In situ δ¹⁸O and Mg/Ca analyses of diagenetic and planktic foraminiferal calcite preserved in a deep-sea record of the Paleocene-Eocene thermal maximum: Paleoceanography, v. 28, p. 517–528, https://doi.org/10.1002/palo.20048.
- Kraus, M.J., and Riggins, S., 2007, Transient drying during the Paleocene–Eocene Thermal Maximum (PETM): Analysis of paleosols in the Bighorn Basin, Wyoming: Palaeogeography, Palaeoclimatology, Palaeoecology, v. 245, p. 444–461, https://doi.org/10.1016/j.palaeo.2006.09.011.
- Lauretano, V., Hilgen, F.J., Zachos, J.C., and Lourens, L.J., 2016, Astronomically tuned age model for the early Eocene carbon isotope events: A new high-resolution δ^{13} C benthic record of ODP Site 1263 between ~49 and ~54 Ma: Newsletters on Stratigraphy, v. 49, p. 383–400, https://doi.org/10.1127/nos/2016/0077.
- Lourens, L.J., Sluijs, A., Kroon, D., Zachos, J.C., Thomas, E., Röhl, U., Bowles, J., and Raffi, I., 2005, Astronomical pacing of late Palaeocene to early Eocene global warming events: Nature,

- v. 435, p. 1083–1087, https://doi.org/10.1038/nature03814.
- McCarren, H.K., 2009, Paleoceanographic variability of extreme climates in the early Paleogene [Ph.D. thesis]: Santa Cruz, University of California Santa Cruz, 196 p.
- Nicolo, M.J., Dickens, G.R., Hollis, C.J., and Zachos, J.C., 2007, Multiple early Eocene hyperthermals: Their sedimentary expression on the New Zealand continental margin and in the deep sea: Geology, v. 35, p. 699–702, https://doi.org/10.1130 /G23648A.1.
- PALAEOSENS Project Members, 2012, Making sense of palaeoclimate sensitivity: Nature, v. 491, p. 683–691, https://doi.org/10.1038/nature11574.
- Pearson, P.N., Shackleton, N.J., and Hall, M.A., 1993, Stable isotope paleoecology of middle Eocene planktonic foraminifera and multi-species isotope stratigraphy, DSDP Site 523, South Atlantic: Journal of Foraminiferal Research, v. 23, p. 123–140, https://doi.org/10.2113/gsjfr.23.2 .123, https://doi.org/10.2113/gsjfr.23.2.123.
- Pearson, P.N., Ditchfield, P.W., Singano, J., and Harcourt-Brown, K.G., 2001, Warm tropical sea surface temperatures in the Late Cretaceous and Eocene epochs: Nature, v. 413, p. 481–487, https://doi.org/10.1038/35097000.
- Penman, D.E., Hönisch, B., Zeebe, R.E., Thomas, E., and Zachos, J.C., 2014, Rapid and sustained surface ocean acidification during the Paleocene-Eocene Thermal Maximum: Paleoceanography, v. 29, p. 357–369, https://doi.org/10.1002 /2014PA002621.
- Roberts, C.D., LeGrande, A.N., and Tripati, A.K., 2011, Sensitivity of seawater oxygen isotopes to climatic and tectonic boundary conditions in an early Paleogene simulation with GISS ModelE-R: Paleoceanography, v. 26, PA4203, https://doi .org/10.1029/2010PA002025.
- Schmitz, B., and Pujalte, V., 2007, Abrupt increase in seasonal extreme precipitation at the Paleocene-Eocene boundary: Geology, v. 35, p. 215–218, https://doi.org/10.1130/G23261A.1.
- Sluijs, A., Schouten, S., Donders, T.H., Schoon, P.L., Röhl, U., Reichart, G.J., Sangiorgi, F., Kim, J.H., Sinninghe Damsté, J.S., and Brinkhuis, H., 2009, Warm and wet conditions in the Arctic region during Eocene Thermal Maximum 2: Nature Geoscience, v. 2, p. 777–780, https://doi.org/10 .1038/ngeo668.
- Spero, H.J., Bijma, J., Lea, D.W., and Bemis, B.E., 1997, Effect of seawater carbonate concentration on foraminiferal carbon and oxygen isotopes: Nature, v. 390, p. 497–500, https://doi.org/10.1038 /37333.
- Stap, L., Sluijs, A., Thomas, E., and Lourens, L., 2009, Patterns and magnitude of deep sea carbonate dissolution during Eocene Thermal Maximum 2 and H2, Walvis Ridge, southeastern Atlantic Ocean: Paleoceanography, v. 24, PA1211, https:// doi.org/10.1029/2008PA001655.
- Stap, L., Lourens, L., van Dijk, A., Schouten, S., and Thomas, E., 2010a, Coherent pattern and timing of the carbon isotope excursion and warming during Eocene Thermal Maximum 2 as recorded in planktic and benthic foraminifera: Geochemistry, Geophysics, Geosystems, v. 11, Q11011, https:// doi.org/10.1029/2010GC003097.
- Stap, L., Lourens, L.J., Thomas, E., Sluijs, A., Bohaty, S., and Zachos, J.C., 2010b, High resolution deep-sea carbon and oxygen isotope records

- of Eocene Thermal Maximum 2 and H2: Geology, v. 38, p. 607–610, https://doi.org/10.1130/G30777.1.
- Tindall, J., Flecker, R., Valdes, P., Schmidt, D.N., Markwick, P., and Harris, J., 2010, Modelling the oxygen isotope distribution of ancient seawater using a coupled ocean-atmosphere GCM: Implications for reconstructing early Eocene climate: Earth and Planetary Science Letters, v. 292, p. 265–273, https://doi.org/10.1016/j.epsl.2009 .12.049.
- Tipple, B.J., Pagani, M., Krishnan, S., Dirghangi, S.S., Galeotti, S., Agnini, C., Giusberti, L., and Rio, D., 2011, Coupled high-resolution marine and terrestrial records of carbon and hydrologic cycles variations during the Paleocene–Eocene Thermal Maximum (PETM): Earth and Planetary Science Letters, v. 311, p. 82–92, https://doi.org/10.1016 /j.epsl.2011.08.045.
- Tripati, A.K., and Elderfield, H., 2004, Abrupt hydrographic changes in the equatorial Pacific and subtropical Atlantic from foraminiferal Mg/Ca indicate greenhouse origin for the thermal maximum at the Paleocene-Eocene boundary: Geochemistry, Geophysics, Geosystems, v. 5, Q02006, https://doi.org/10.1029/2003GC000631.
- van Hinsbergen, D.J., de Groot, L.V., van Schaik, S.J., Spakman, W., Bijl, P.K., Sluijs, A., Langereis, C.G., and Brinkhuis, H., 2015, A paleolatitude calculator for paleoclimate studies: PLoS One, v. 10, e0126946, https://doi.org/10.1371/journal .pone.0126946.
- Westerhold, T., Röhl, U., Laskar, J., Raffi, I., Bowles, J., Lourens, L.J., and Zachos, J.C., 2007, On the duration of Magnetochrons C24r and C25n, and the timing of early Eocene global warming events: Implications from the ODP Leg 208 Walvis Ridge depth transect: Paleoceanography, v. 22, PA2201, https://doi.org/10.1029/2006PA001322.
- Westerhold, T., Röhl, U., Donner, B., McCarren, H.K., and Zachos, J.C., 2011, A complete high-resolution Paleocene benthic stable isotope record for the central Pacific (ODP Site 1209): Paleoceanography, v. 26, PA2216, https://doi.org/10.1029/2010PA002092.
- Zachos, J.C., Wara, M.W., Bohaty, S.M., Delaney, M.L., Rose-Petrizzo, M., Brill, A., Bralower, T.J., and Premoli-Silva, I., 2003, A transient rise in tropical sea surface temperature during the Paleocene-Eocene Thermal Maximum: Science, v. 302, p. 1551–1554, https://doi.org/10.1126/science.1090110.
- Zachos, J.C., Schouten, S., Bohaty, S., Quattlebaum, T., Sluijs, A., Brinkhuis, H., Gibbs, S.J., and Bralower, T.J., 2006, Extreme warming of midlatitude coastal ocean during the Paleocene-Eocene Thermal Maximum: Inferences from TEX86 and isotope data: Geology, v. 34, p. 737–740, https://doi.org/10.1130/G22522.1.
- Zeebe, R.E., Zachos, J.C., and Dickens, G.R., 2009, Carbon dioxide forcing alone insufficient to explain Palaeocene–Eocene Thermal Maximum warming: Nature Geoscience, v. 2, p. 576–580, https://doi.org/10.1038/ngeo578.

Manuscript received 25 August 2017 Revised manuscript received 21 November 2017 Manuscript accepted 21 November 2017

Printed in USA